



Robust neural decoding for dexterous control of robotic hand kinematics

Jiahao Fan ^a, Lufis Vargas ^b, Derek G. Kamper ^b, Xiaogang Hu ^{a,c,d,e,f,*}

^a Department of Mechanical Engineering, Pennsylvania State University, University Park, USA

^b Joint Department of Biomedical Engineering, University of North Carolina at Chapel Hill and North Carolina State University, USA

^c Department of Kinesiology, Pennsylvania State University, University Park, USA

^d Department of Physical Medicine & Rehabilitation, Pennsylvania State Hershey College of Medicine, USA

^e Huck Institutes of the Life Sciences, Pennsylvania State University, University Park, USA

^f Center for Neural Engineering, Pennsylvania State University, University Park, USA



ARTICLE INFO

Keywords:

Hand function

Hand dexterity

Neural decoding

Robotic hand

Joint kinematic control

ABSTRACT

Background: Manual dexterity is a fundamental motor skill that allows us to perform complex daily tasks. Neuromuscular injuries, however, can lead to the loss of hand dexterity. Although numerous advanced assistive robotic hands have been developed, we still lack dexterous and continuous control of multiple degrees of freedom in real-time. In this study, we developed an efficient and robust neural decoding approach that can continuously decode intended finger dynamic movements for real-time control of a prosthetic hand.

Methods: High-density electromyogram (HD-EMG) signals were obtained from the extrinsic finger flexor and extensor muscles, while participants performed either single-finger or multi-finger flexion-extension movements. We implemented a deep learning-based neural network approach to learn the mapping from HD-EMG features to finger-specific population motoneuron firing frequency (i.e., neural-drive signals). The neural-drive signals reflected motor commands specific to individual fingers. The predicted neural-drive signals were then used to continuously control the fingers (index, middle, and ring) of a prosthetic hand in real-time.

Results: Our developed neural-drive decoder could consistently and accurately predict joint angles with significantly lower prediction errors across single-finger and multi-finger tasks, compared with a deep learning model directly trained on finger force signals and the conventional EMG-amplitude estimate. The decoder performance was stable over time and was robust to variations of the EMG signals. The decoder also demonstrated a substantially better finger separation with a final predicted error of joint angle in the unintended fingers.

Conclusions: This neural decoding technique offers a novel and efficient neural-machine interface that can consistently predict robotic finger kinematics with high accuracy, which can enable dexterous control of assistive robotic hands.

1. Introduction

The human digits are capable of performing precise, coordinated movements with little conscious effort. Neuromuscular injuries, on the other hand, can lead to impairment of the hand function, limiting community living. A number of assistive devices, such as prosthetic hands or exoskeleton gloves, have been developed to restore impaired or lost hand functions [1–4]. However, the translation of these robotic devices has been limited. One major limiting factor is the lack of a robust neural-machine interface that can reliably translate the user's intended motions to control these multi-degree-of-freedom (DoF) devices. Particularly for the hand, an accurate decoding of individual finger

movements remains a long-standing challenge.

For individuals with voluntary muscle activation capability, surface electromyography (EMG) has been widely used for motor intent detection for the control of assistive devices [5–7]. Typically, pattern recognition is used to classify a finite set of intended movements [8–11], or the movement of a specific joint is made proportional to EMG features (such as EMG amplitude) [12–14]. These global EMG-based control strategies are sensitive to interference. For example, the EMG amplitude can be biased by varying distances and tissue types located between the target muscle and the surface electrode. EMG signals can also be contaminated by motion artifacts and crosstalk of multiple muscles in close proximity [15,16]. All of these interferences can limit robust

* Corresponding author. Pennsylvania State University, University Park 205 Reber Building, University Park, PA, 16802, USA.

E-mail address: xuh120@psu.edu (X. Hu).

control of robotic devices. Consequently, the stability and accuracy of such control strategies is not satisfactory, thereby limiting robust dexterous control of robotic hands.

Alternatively, motoneuron firing activity can also be used as a neural interface [17]. The frequency/probability of the motoneuron firing at the population level can directly reflect the neural drive from the brain to the muscles. Essentially, the spinal cord output signal (firing events) can be used to decode the spinal input signal (motor command from the brain). The decoded neural drive signal can be more robust for decoding motor intent than global EMG activities, because the binary firing events are less susceptible to noise than measuring analog EMG features. Currently, motoneuron firing events are extracted through motor unit (MU) decomposition of high-density sEMG (HD-EMG) recordings, which separates the superimposed action potentials into individual motoneuron firing activities [18–23]. Different real-time MU decomposition algorithms have shown great promise for neural decoding purposes [24, 25]. Nevertheless, one drawback of the decomposition approach is the high computational intensity and computational inefficiency associated with the extraction of individual MU firing activity. Namely, spikes of individual MUs are extracted, and these firing events are then merged to represent the population neuron firing behavior. Essentially, information of firing rates of individual MUs, extracted from the most computational steps of the decomposition, is not utilized.

Accordingly, the purpose of the current study was to develop a robust and efficient neural decoder that can continuously decode the motor intent of individual fingers, feasible for dexterous and continuous control of robotic hands in real-time (Fig. 1). We implemented a deep neural network model to establish continuous mapping from global EMG features to population motoneuron firing frequency for individual finger muscles, without the intermediate process of MU decomposition. While MU decomposition was used to label annotations for offline model training, the trained model could continuously predict the neural signals for real-time prosthetic control without MU decomposition. Recently, deep neural network models, such as convolutional neural networks (CNNs) and recurrent neural networks (RNNs), have been used for neural signal processing. For example, in the context of sEMG-based gesture classification, accurate pattern classification can be achieved using multi-stream CNNs [26,27]. Inter-person recognition of hand gestures is also feasible after fine-tuning the network parameters [28]. Moreover, there has also been a growing body of work that explored deep learning techniques for the continuous estimation of dynamic movements. For instance, an earlier work utilized CNN to establish a regression-based decoding of wrist movements [29]. Geng et al. [30] developed a CNN-attention network to predict joint angles during hand grasping movements. Studies have also employed long-short term memory networks to predict continuous finger movements [31–33]. Collectively, these studies implemented deep learning models to learn a direct mapping between EMG signals and motor output (fingertip force

or joint kinematics). It is unclear whether the model trained on one type of motor output can be generalized to the other type (e.g., models trained on force may not generalize well in joint kinematic prediction). Recently, we have also established a generic CNN model for accurate decoding of fingertip forces [34]. The results showed that the CNN-based decoder demonstrated similar decoding accuracy compared with the MU-decomposition based approach. However, the CNN model was not finger specific and can only predict one finger output at a time.

To address these issues, we first established a generalized model specifically trained on subject cohorts, and the model was then personalized to individual subjects for decoding of individual finger kinematics, with the target finger and the joint angles predicted simultaneously. Finally, the decoder was evaluated for the control of a multi-DoF robotic hand. Our results showed that the developed decoder could accurately predict the users' finger kinematics, and could consistently control the robotic hands to the desired joint angles over time, with minimal movements occurred in the undesired fingers, comparing with a EMG amplitude approach and a CNN model directly trained on force signals.

The research framework is visualized in Fig. 1. The main contribution of this paper was two-fold: (1) We developed a novel neural decoder that can directly learn the motoneuron firing frequencies from global EMG features. Different from MU decomposition approaches, we obtained the population firing information directly from EMG features without the need for decomposing individual MU activities after model training. As a result, our approach is highly efficient for offline implementations. (2) We implemented the neural-drive-based independent control of single-finger and multi-finger movements of robotic hand in real-time. We demonstrated that the neural-drive information could lead to high performance, real-time prostheses control. Compared with the conventional global EMG amplitude-based and deep learning-based approaches, our method shows superiority in accuracy, robustness, and finger isolation during real-time prostheses control.

2. Methods

A. Participants

Ten neurologically intact participants (three females and seven males, age: 23–36) were recruited for this study. Prior to the experiment, all participants were given informed consent via protocols (#16-0801) approved by the University Institutional Review Board.

B. Experimental Protocol

The experiment was composed of repetitive dynamic finger flexion and extension tasks. During data acquisition, subjects were seated in front of a desk with their right forearm in the neutral position supported

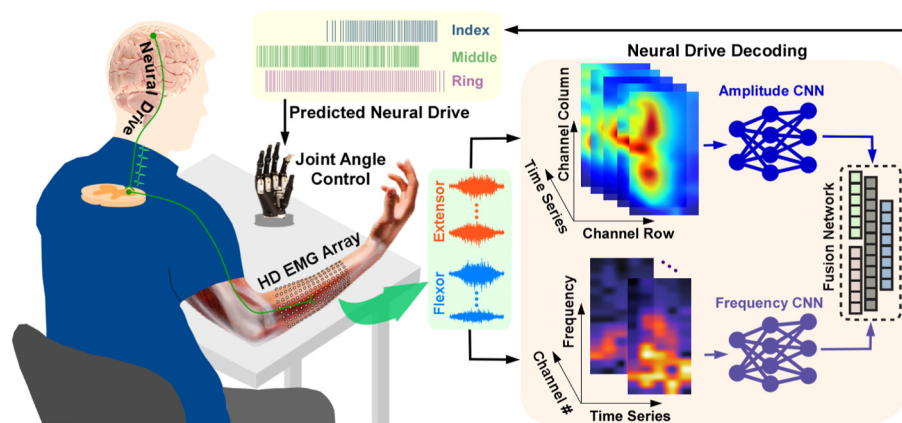


Fig. 1. Overview of the research framework. High-density electromyographic (HD-EMG) signals were obtained from the extrinsic finger flexor and extensor muscles. Convolutional neural network (CNN)-based models were used to learn the mapping from HD-EMG amplitude and frequency features to finger-specific neural drive signals (i.e., population neuron firing frequency). The predicted neural drive signals were then used to continuously control the joint angles of the index, middle, and ring fingers of a prosthetic hand.

by a large foam pad, with a fixed wrist angle. After skin preparation, two 8 × 16 HD-EMG electrode grids (a 3-mm recording diameter for each electrode and an inter-electrode distance of 10 mm) (OT Bioelectronics) covered the anterior and posterior sides of the forearm to record EMG signals of extrinsic finger flexor and extensor muscles. The electrode grid was placed based on palpation of the targeted muscles. The biosignal amplifier EMG-USB2+ (OT Bioelectronics) was used to sample the EMG signals at 2048 Hz with a gain of 1000 and band-pass filtered at 10–900 Hz. Kinematics of the metacarpophalangeal (MCP) joints of the index, middle, and ring fingers were recorded using a custom-made sensor glove, and the MCP angle data were sampled at 100 Hz.

During the experiment, subjects extended and flexed one designated finger (one of index, middle, and ring fingers) or three fingers concurrently, following a target trajectory comprised of half-sine waves (Fig. 2B), ranging from 0% (full extension) to 100% (full flexion) range of motion (ROM). The finger movements were repeated four times within each trial for 10 s, and eight trials were performed. Overall, a total of 32 dynamic movements (4 finger patterns × 8 trials) were recorded for each subject. The first 3 trials were used for CNN model refinement, 1 trials were used for validation, and the remaining 4 trials were used to construct the regression functions (Fig. 2C) between the predicted neural drive and the measured joint angles of each finger. Lastly, to test the decoder performance, the participants controlled the prosthetic finger joints using the predicted joint angle based on the regression function (Fig. 2D). They produced different finger flexion and extension movements from 0% to 100% ROM with 4 repetitions in 16 s, using either one of the three fingers or three fingers concurrently (Fig. 2E). A different movement velocity was used to evaluate the generalizability of the neural network decoder.

C. Neural Decoder

Feature Extraction: Two types of features, termed the amplitude map and the frequency map, were extracted from raw EMG recordings before fed into the network. The 128-channel HD-EMG recordings were first segmented into a sequence of 96-samples (46.88 ms) with a step size of 64 samples (31.25 ms). Five consecutive segments were used to overlap the temporal information between segments. The amplitude map was extracted by computing the root-mean-square (RMS) value of each channel separately in each signal segment. The 128 RMS values were then rearranged into a 16 × 8 (height × width) map as the original electrode grid spatial layout (see in Fig. 1). The amplitude maps from five consecutive windows were stacked to a 3-dimensional tensor $F_{amp} \in \mathbb{R}^{T \times H \times W}$ (Time × Spatial × Spatial), where $T = 5$, $H = 16$, and $W = 8$. Likewise, the frequency map was extracted via Fast Fourier Transform separately on each 128-channel on each segment, resulting in the frequency feature $F_{spec} \in \mathbb{R}^{N \times M \times T}$ (Spatial × Frequency × Time), where $N = 128$, $M = 49$, and $T = 5$.

Data Labelling: To label the EMG data for supervised learning, we used offline state-of-the-art MU decomposition method, the fast independent component analysis (FastICA) method [21,22] to extract the

times of individual motor units (MUs). The pseudocode of the algorithm is shown in the Supplementary material. Briefly, the raw EMG signals were first extended by an extension factor ($f_e = 10$) and whitened. The separation vectors and associated signal sources representing individual MU information were obtained via a fixed-point iteration algorithm [21,23,35]. The binary firing events of individual MU were separated from the background signal sources through a binary classification using the Kmeans++ algorithm [36,37]. A modified 'silhouette distance' (SIL) measurement [38] was used to quantify the separation quality of the source signals, where source signals with low SIL values (<0.6) were excluded from the MU pool. The refined binary firing activities were further summed to a single composite train, from which the population firing frequency of the MU pool can be obtained. The population firing frequency was then normalized via min-max normalization, the normalized firing frequency was then scaled up by a factor of 15, and categorized and labeled into 16 classes ranging from 0 to 15. Inherently, label 0 corresponds to the obtained lowest firing frequency and label 15 corresponds to the highest firing frequency.

Neural network: We used a multi-scale-view convolutional neural network (CNN) to extract high-level representations from global EMG features. The network consists of two branches, termed the frequency domain branch and the time domain branch, respectively (see in Supplementary Materials, Table S1). Therefore, the frequency domain branch enabled the exploration of the correlation of frequency spectrums between time frames. By shifting the kernel ($\omega \in \mathbb{R}^{N \times p \times q}$) pixel by pixel across the input frequency feature (Equation (1)), where F_{spec} refers to the frequency spectrum feature map, Y is the output intermediate feature map, and f_{ij} are the coordinates indicating the location of the kernels on the input feature. Because action potentials in HD-EMG signals could arrive at different channels at different times, the third dimension of the kernels explored the spatial-frequency

$$Y_{ij} = \sum_{a=0}^{N-1} \sum_{b=0}^{q-1} \omega_{ab} F_{spec}(i+a)(j+b) \quad (1)$$

Likewise, the time-domain branch was used to extract the information from the amplitude feature. The kernels ($\nu \in \mathbb{R}^{T \times p \times q}$) were encouraged to template matching the activated regions on the EMG amplitude maps, which could be formulated as Equation (2), where F_{amp} refers to the amplitude feature map, Z is the output representation map, and f_{ij} are the coordinates indicating the location of the kernels on the input feature.

$$Z_{ij} = \sum_{a=0}^{T-1} \sum_{b=0}^{q-1} \nu_{ab} F_{amp}(i+a)(j+b) \quad (2)$$

Since the localized activation regions on the amplitude features were associated with individual finger movements, the network could potentially learn the mapping between the EMG features produced by different finger muscle compartments and the population firing frequency of individual fingers. By providing a sequence of consecutive EMG features in different time frames to the network, the transition

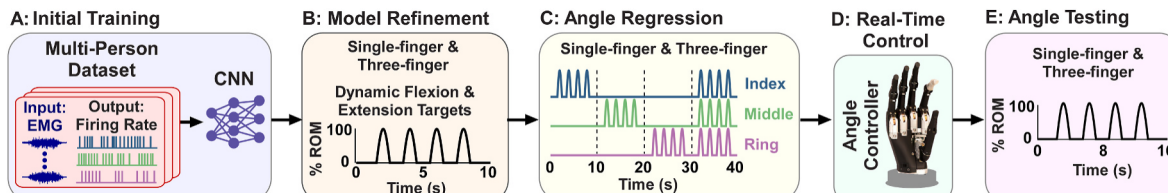


Fig. 2. Neural network model for real-time control of prostheses. A: Initial training of the neural network using a large dataset to establish a generic mapping from EMG features to population firing frequency. B: The CNN model parameters were refined using subject specific data from dynamic single- and multi-finger movement tasks. The MCP joints started from full extension (0% ROM), and flexed to 100% ROM, and extended back to 0% ROM. C: Perform a quadratic regression to convert population firing frequency to joint angle. Data from the single- and multi-finger movement tasks were used for the regression. D: Real-time control of a prosthesis using the CNN model prediction through an angle controller. E: Testing of the angle prediction performance using data from the single- and multi-finger movement tasks (0–100% ROM).

ruples of sEMG features over ttime fis also taken into consideration.

The high-level representations yielded by the two branches were flattened and concatenated. Two fully connected layers were used for feature fusion. At last, three output layers were used in parallel to predict the population MU firing frequencies generated by the index, middle, and ring fingers concurrently. Specifically, each output layer in charge of predicting the firing frequencies of the current input EMG features were produced by the muscle contraction of one of the three fingers. The final output of each output layer is a 16-dimensional vector, in which each element represents the probability (after softmax operation) of the predicted firing frequency. The predicted firing frequency was identical to the input class label (defined as the normalized discrete firing frequencies ranging from 0 to 15).

Let y_j^i denotes the labeled class of $f_i \in \{0, 1, 2\}$ referring to the index of individual fingers, and $j \in \{0, 1, 2, \dots, 15\}$ refers to the class of the firing frequency. p_j^i denotes the corresponding predicted probability. We applied the Cross Entropy Loss between the target labels and predicted probabilities, which is a summation of all the three output layers (Equation (3)):

$$L = \sum_{o} \sum_{i} \sum_{j} y_j^i \log p_j^i \quad (3)$$

where O represents each observation, D and C represent the total account of output layers (number of fingers) and firing frequency classes, respectively.

D Neural Decoder Training

Initial training: The initial training established a generic mapping from EMG features to population firing frequency of individual fingers. We used a dataset of isometric finger force tasks from a series of earlier studies [24,39,40] to train the neural network (Fig. 2A). These datasets encompassed a range of scenarios, including EMG recordings when subjects performed isometric flexion/extension force of individual fingers. Additionally, the datasets included recordings while subjects performed multiple finger dynamic movements, either sequentially [39] or concurrently [40]. The firing frequency of each finger was obtained by summarizing the firing events of individual MUs grouped by fingers. The obtained firing frequency was labeled and served as the target class for supervised training. One trial of data was held out for validation. The network weights were updated for 1500 iterations using Adam Optimizer [41] to minimize L . The model with the highest validation score (defined as the average correlation coefficient between the predicted firing frequencies and the measured forces of the index, middle, and ring fingers) was selected for subsequent applications.

Model fine-tuning: After the neural decoder was trained on HD-EMG signals when subjects performed isometric force tasks, it is essential to enhance the performance on predicting dynamic finger movements for dexterous robotic hand control. The joint angle decoding performance without this refinement is shown in Fig. S1 in the supplementary material. Therefore, we fine-tuned the neural decoder using data obtained from the current study involving finger dynamic movements. In particular, the network was personalized to each subject by fine-tuning the network weights using the first 3 trials from each subject, with 1 trial held out for validation. The network was trained for 80 iterations, the network weights that yielded the best validation score were selected for further application.

Joint angle prediction: To predict joint angle using the refined model, we set up a regression function. First, the firing frequency predicted by the neural decoder was smoothed by a moving average filter (500 ms window with a moving step of 31.25 ms). The smoothed firing frequency was further filtered by a Kalman filter [24]. As a result, the smoothed firing frequencies were updated every 31.25 ms (32 Hz) for the three individual fingers concurrently. 32 Hz was chosen because the data

packet can be obtained from the acquisition system was filtered at 32 Hz. We used a quadratic regression over linear regression based on an earlier study [42]. We built three bivariate quadratic regression models using the last four trials of each subject from the current study (Fig. 2C), to predict MCP angles of the three fingers based on the smoothed firing frequency.

The regression function is

$$J_i(t) = a_{f_i} D_{f_i}(t) + b_{f_i} D_{f_i}^2(t) - c_{f_i} D_{f_i}(t) + d_{f_i} D_{f_i}^2(t) + C_i \quad (4)$$

$\begin{matrix} \text{neural drive} & - & \text{neural drive} & - & \end{matrix}$
 $\begin{matrix} \text{terms for flexor} & & \text{terms for extensor} & & \end{matrix}$

Where J_i represents the estimated joint angle for the i -th finger, $D_{f_i}(t)$ is the neural drive signals of flexor muscle, and $D_{f_i}(t)$ is the neural drive signals of the extensor muscle. The coefficients $a_{f_i}, b_{f_i}, c_{f_i}, d_{f_i}$ and C_i represent the regression coefficients. This regression allowed us to establish a relation between the resulting joint angle of each finger and the measured EMG amplitude or the population firing rate of the flexor and extensor muscles.

Real-time prosthetic control: To evaluate the performance of the neural encoder for real-time prosthetic control, real-time decoding of intended joint angles were performed on HD-EMG signals when subjects performed dynamic MCP flexion and extension tasks (Fig. 2D and E). The predicted angles of the CNN method were used to control the MCP joint of the index, middle, and ring fingers of the prosthetic hand (i-Limb, Ossur) through a custom MATLAB (MathWorks Inc) interface. Supplementary video S1 demonstrated the real-time joint kinematic control of the prosthetic hand. Three angle sensors were fixed on the prosthetic fingers to record the MCP joint angles. The angle information was sent to a custom-made proportional derivative (PD) controller as feedback signals to control the MCP angle of each of the three fingers of the prosthetic. The controller updated the reference angle at a rate of 8 Hz, while motor commands were updated at a rate of 32 Hz.

Supplementary video related to this article can be found at <https://doi.org/10.1016/j.combiomed.2023.107139>

As a comparison with the neural network decoder, we also performed angle prediction using a EMG amplitude method [43] (termed EMG method). First, the top 60 channels with the highest RMS value out of the 128 EMG channels were selected separately for the flexor and extensor muscles. The EMG data during the activation of individual intended fingers were used for the channel selection. Second, because of EMG activities associated with inevitable activation of unintended fingers, some of the selected top 60 channels could represent motor output of unintended fingers. This could lead to false positive errors in motor output predictions of intended fingers. To address this issue, we performed a channel refinement procedure to further remove channels with potential EMG recordings (i.e., cross-talk) of unintended fingers. Specifically, the EMG amplitude (RMS) was calculated using the moving average filter (500-ms window with a moving step of 31.25 ms) for the individual 60 channels. A regression analysis was then performed between the EMG amplitude and different finger angles during dynamic movement tasks. If the coefficient of determination (R^2) value with the intended fingers were higher than with the other two fingers, the given EMG channel was refined. Otherwise, the channel was removed. The assumption was that the EMG channel with muscle activities associated with a given finger should have a high correlation with the motor output of that finger. Finally, the RMS values of the refined EMG channels were calculated using the same moving average filter method and averaged across channels for each finger. The same Kalman filter was applied to the average RMS values. Three bivariate quadratic functions for the EMG method were constructed using data from the angle regression trials.

In addition, to highlight the benefit of utilizing neural drive signals, we conducted a comparative analysis between our neural drive method and a similar CNN approach that directly used the force signals as the

target. The rational behind this comparison was that EMG features were correlated with both kinematic and kinetic variables. Therefore, the knowledge learned from the force prediction task could be transferred to the joint angle prediction task. To ensure a fair comparison, we used the same network architecture and training parameters as in the neural drive signal approach. The only difference was that the training target was the normalized discrete force values during the initial training phase. By doing so, we were able to evaluate the performance difference achieved by incorporating neural drive signals in contrast to directly using kinematic and kinetic variables. To ensure clarity, we used the term CNN method to refer to the neural drive method unless stated otherwise. In cases where both CNN methods were mentioned, CNN-force (CNN-F) represented the CNN method pre-trained using the force values, while CNN-neural-drive (CNN-ND) represented the CNN method pre-trained using the neural drive signals.

E. Statistical Analysis

The performance of the joint angle prediction was evaluated by the root mean squared error (RMSE) and coefficient of determination (R^2) values between the actual measured angles and the predicted angles. To quantify finger isolation of the decoding, both intended and unintended fingers were evaluated in the single-finger tasks. Repeated measures analysis of variance (ANOVA) was performed on the dependent variables. A pairwise comparison was conducted using the Bonferroni method when necessary. The significance level α was set as 0.05. To further quantify finger isolation, we also categorized the fingers into active and rest states based on the predicted angle in the single-finger tasks. Predicted angle sequences were categorized into active or rest states based on an output threshold of 10% ROM. The results based on 5% and 15% ROM thresholds were also reported in Fig. S2 of the supplemental material. In a given time, if the angle of a finger was above the threshold, the corresponding finger was categorized as active. The percentages of output data samples in different finger combination categories were also reported. A high percentage only in the single intended finger category was considered a better finger isolation than a high percentage in the multi-finger categories.

3. Results

To quantify the decoding performance of joint kinematics, we calculated the RMSE between the measured angle around the metacarpophalangeal (MCP) joints and the predicted angle (either from CNN method or EMG method). The supplemental video S1 demonstrated the real-time decoding using the CNN method and continuous control of

single and multiple fingers of a prosthesis. Fig. 3 depicts the performance of joint angle prediction using the CNN-based methods (CNN-ND and CNN-F) and the EMG-amplitude estimates. The decoding performance in the single-finger joint movement task is shown in Fig. 3. An example trial of the ring finger flexion-extension task is illustrated in Fig. 3A. The CNN-ND method showed a better angle prediction performance in comparison with the CNN-F method and the EMG method. The CNN-ND method also revealed an underestimation of the joint angle in the unintended fingers, whereas the EMG method demonstrated an overestimation of the joint angle. Fig. 3B illustrates the average prediction errors of the intended fingers across subjects. The two-way (*method* (CNN-ND vs. CNN-F vs. EMG) \times *finger* (index vs. middle vs. ring)) ANOVA revealed a significant difference ($F(2,27) = 13.43$, $p < 0.001$) in the RMSE values obtained by different methods with no significant interaction effect between the *method* and *finger*. Overall, the CNN-ND method achieved the lowest RMSE value in most cases, except in the ring finger condition.

We also evaluated the predicted movement errors of the unintended fingers. Since the unintended fingers were supposed to produce no joint movement, a zero-degree angle movement was considered the ground-truth of the unintended fingers. Accordingly, the RMSE of the unintended fingers was calculated between zero-degree angle and the actual or predicted angles. The RMSE between zero-degree angle and the actual angle (or the predicted angles) were calculated (Fig. 3C). The ANOVA showed that the factor of *method* ($F(2, 27) = 65.90$, $p < 0.001$) had a significant effect on the RMSE with no interaction effect with the *finger* factor. The pairwise comparison showed that the RMSE of the CNN-ND method was significantly lower than that of the CNN-F method ($p < 0.001$), the EMG-amplitude method ($p < 0.001$), and the actual joint angle ($p < 0.001$), indicating that the CNN-ND method can better predict intended movement of the subjects than the actual movement. Overall, the CNN-ND method showed least amount of finger-crosstalk with the best finger isolation.

We then quantified the active vs. rest states of the fingers based on the predicted joint angles (Fig. 4). In a given time, if the angle of a finger was above the 10% range of motion (ROM) threshold, the finger was considered active. Most of the predicted joint angles of the CNN method were categorized into the active intended fingers, with most of the angle of the unintended fingers categorized into a rest state. In contrast, angles predicted by the EMG-amplitude method was largely affected by the activation of the intended finger and one or multiple unintended fingers, with the highest percentage observed in the three-finger IMR active state regardless the intended finger. This indicates the poor ability of finger isolation of the EMG-amplitude method. The results based on the 5% and 15% ROM thresholds are also reported in Fig. S2 in the

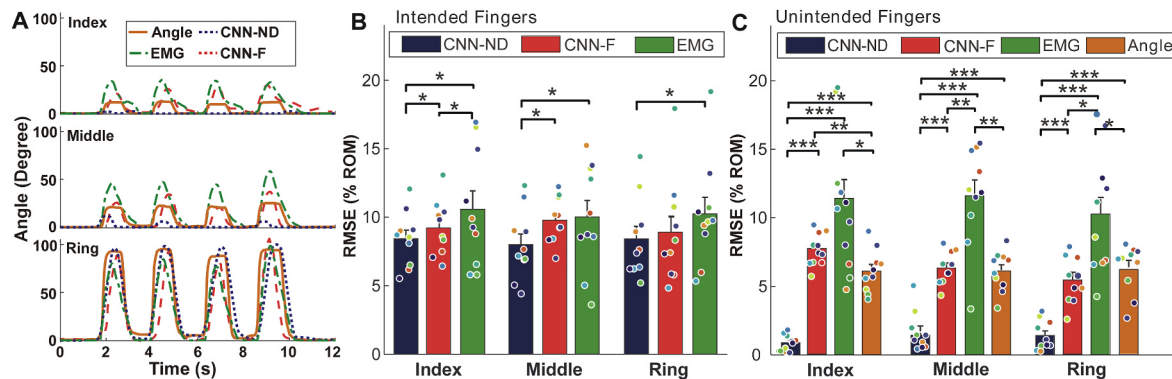


Fig. 3. Prediction of individual finger joint angles using the CNN and EMG methods. CNN-ND represents the CNN model pre-trained by the neural drive signals, and CNN-F represents the CNN model pre-trained directly by the normalized force signals. A: An example trial of the joint angle prediction, when the ring finger was instructed to flex and extend while other fingers relaxed. Zero-degree means full extension. The RMSE of individual fingers was shown for the intended (B) and unintended (C) fingers. The range of motion (ROM) was normalized by the maximum flexion angle of individual fingers. Filled circles of the same color represent the same subject. Error bars represent standard error. *, $p < 0.05$. **, $p < 0.01$. ***, $p < 0.001$.

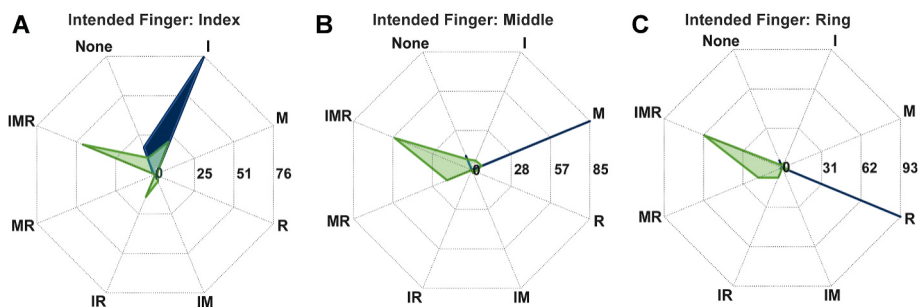


Fig. 4. Active finger classification of the CNN method (blue) and the EMG method (green). I, M, and R represent index (A), middle (B), and ring (C) fingers, respectively. Predicted angle time series of the three fingers were categorized into active or rest states based on a 10% ROM threshold. The radius of the plot represents the percentage of force data samples in each category, with different contour lines representing different percentage values.

supplemental material.

The decoding performance in the multi-finger movement task is shown in Fig. 5. An exemplar trial comparing the actual and predicted joint angles is shown in Fig. 5A during the initial regression. The results indicated that both CNN and EMG-amplitude methods could accurately predict joint angles of the three fingers in the initial regression phase. An exemplar trial during the subsequent testing is shown in Fig. 5B. The predicted angle of the CNN method still fits the actual measured joint angle accurately. In contrast, the prediction error of the EMG-amplitude method across the three fingers increases sharply in the testing phase, especially at the peak flexion angles. The two-way (method (CNN vs. EMG) \times phase (initial regression vs. testing)) repeated measures ANOVA showed that both the method ($F(1,9) = 14.966$, $p = 0.004$) and the phase ($F(1,9) = 6.629$, $p = 0.030$) had a significant influence on the RMSE (Fig. 5C) with no interaction ($p > 0.05$). The pairwise comparison revealed that the RMSE of the EMG-amplitude method during the testing phase was significantly higher than that of the EMG method during the initial regression ($p < 0.05$). In contrast, the RMSE of the CNN method did not increase significantly during the testing phase, compared with the initial regression ($p > 0.05$). This indicated that the CNN method

was more stable and robust than the EMG method against interference over time. We also quantified the angle prediction performance during testing (Fig. 5D and E). The one-way repeated measures ANOVA showed that the RMSE (Fig. 5D) of the CNN method was significantly lower than that of the EMG method ($F(1,9) = 13.071$, $p = 0.006$). Likewise, the R^2 (Fig. 5E) of the CNN method was also significantly higher than that of the EMG-amplitude method ($F(1,9) = 6.892$, $p = 0.028$).

Finally, the computation efficiency was also estimated to ensure the usability of the proposed methods. The computational latency was 37 ms (16 ms delay from retrieving data packet, up to 3 ms for signal pre-processing, up to 11 ms for neural decoding, and 7 ms for regression and filtering) using GPU Nvidia GTX 1660, CPU Intel Core i7-9700, and Memory of 24 GB. This delay is well below the acceptable loop delay (100–150 ms) in human-robot interactions [44,45].

4. Discussion

This study developed a robust and efficient neural decoding method that can predict joint angles of individual finger, which is promising for real-time dexterous control of a robotic hand. The CNN mapped hand-

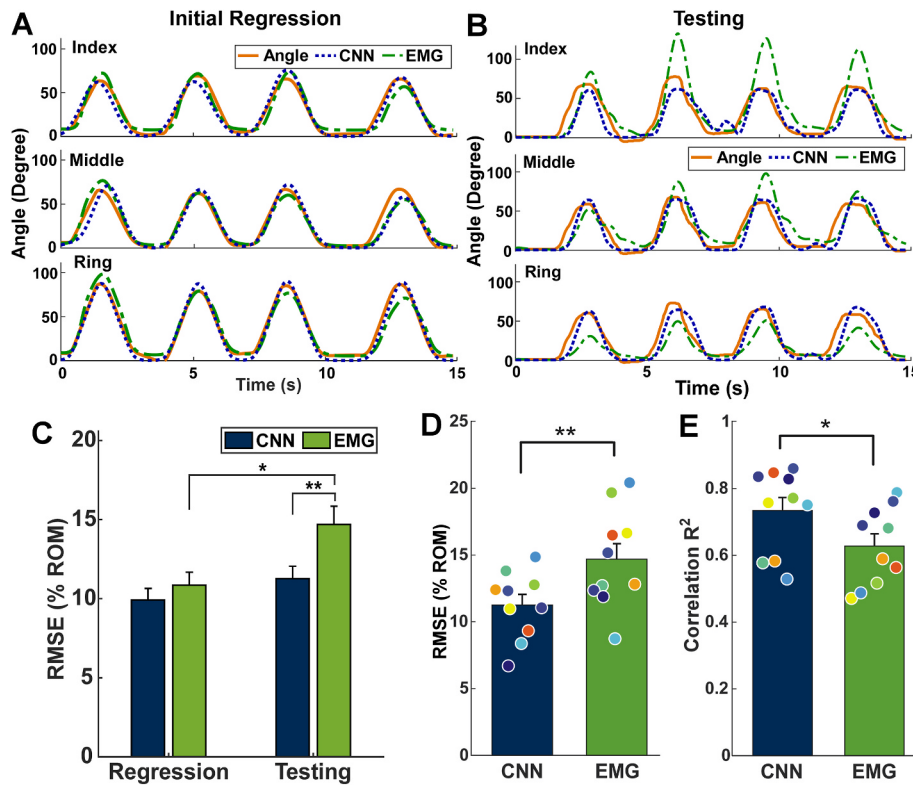


Fig. 5. Prediction of multi-finger joint angles concurrently using the CNN and EMG methods. A: An exemplar trial of multi-finger joint angle prediction of the CNN and EMG methods during initial regression. B: An example trial of angle prediction of the CNN and EMG methods during subsequent testing. C: A comparison of the initial regression and testing of the two methods. The averaged RMSE (D) and coefficient of determination (E) of the two methods during subsequent testing. Filled circles represent individual subjects. Error bars represent standard error. *, $p < 0.05$. **, $p < 0.01$.

crafted HD-EMG features to popuflatfion neuron ffirfing frequency (i.e., neuralf drfive) specific to findividufl ffingers durfing sfingle-finger and mufltfi-ffinger movements. Because EMG features have a more dfirect refelation wfh MU ffirfing activfity than wfh jofint kfinematsics, we trafined the modefl on popuflatfional neuron ffirfing frequency. Thhis afferflowed us to ffirf the estabflfish a generic modefl trafined on data from one type of task (e.g., isometric force task), and the modefl can be generalfized to dynamfc movement tasks after network parameter reffinement. In addfition, the modefl performance and ffamfing rate further improved by usfing hand-crafted features of ampfitude and frequency maps of EMG for the network modefl finput. We aalso impflemented an effficient, two-step network trafining strategy (i.e., an inter-subject finitifial trafining and a subsequent subject-specific modefl reffinement on dynamfc finger movement tasks), whfch enabfled an effficient feature mappfing from EMG to neuralf drfive sfignals. The decodfing of neuralf drfive based on popuflatfion neuronalf ffirfing activfity has demonstrated robust decodfing performance, wfh consfistent jofint kfinematic predfictfion accuracy across ffingers and over ttime. In contrast, the performance of the EMG-amplfitude method refealed hffiger error in both sfingle-finger and mufltfi-ffinger tasks. In addfition, the performance of EMG-amplfitude-based decoder aalso degraded over ttime, wfh sharp fincrease in predfictfion error from the finitifial regression phase to testfing phase. The outcomes suggest that popuflatfion neuron decodfing offers a robust and effficient method for continuous motor fintent detectfion of findividufl ffingers. The continuous motor fintent decodfing at the findividufl finger level sheds lights upon dexterous control of assfisfive robotic hands.

The CNN-based neuralf drfive decoder aalso demonstrated its superiforty in finger movement ifosflatfion, wfh mifinal angle predfictfion error on unintended ffingers. Intent detectfion of findependent finger movements has been a long-standing fissue, because of our flfimfited abffity to activate findividufl finger muscle compartments [46,47] and chafiflenges in ifoslated surface EMG recordfings of small muscle compartments [15, 48]. Indeed, the HD-EMG ampfitude method showed substantiafl false positive error in the unintended ffingers, despite a channelf selecfion procedure based on jofint movements of the desired ffingers. Thhis false positive error is present in both categorifical results (wfh sfingle finger movements classififed as aifl-three finger movements) and in angle predfictfion errors (RMSE). Aiflthough channelf selecfion/reffinement can reduce the impact of cross-taflk to some degree [43], the EMG sfignals can still contain substantiafl activfity from other muscle compartments, especiaflly durfing dynamfc finger movements.

In contrast, the decodfing of neuralf drfive usfing neuralf network modefls can accurately detect finger jofint angles in both sfingle-finger and mufltfi-ffinger tasks, wfh predicted movements of the unintended ffingers controffled in a low level. In fact, the predicted jofint angle was even flower than the actual measured jofint angle in the unintended ffingers from the data glove. Thhis is benefiafl from a motor fintent detectfion perspective for robotic control, in that the decoded jofint movements from neuralf drfive dfirectly reflect the movement fintentfion rather than the actualy produced movements. The underestfimation of jofint angle in the unintended ffingers can arise from several factors. Ffirst, the surface HD-EMG gfid on the forearm only captured activfities of the extifnsic muscles near the skin surface. Activfities of the ifinifnsic finger muscles in the hand and the flexor dfigitorum profundus were not recorded, whfch could contribute to the actual movement of the MCP jofint in the undesired ffingers. Second, it is wffl known that there is coordinated movement among ffingers that flfimfif finger findependent. Mechanicafl couplfing from the tendifnous structure and skin connectfions across ffingers [46,49] is one factor that leads to these coordinated finger movements. Nevertheless, thhis mechanicafl couplfing effect was not factored in the CNN modefl.

The current study focused on the decodfing of fintended movements of findividufl ffingers, and the decoder performance was vaflidated on the real-ttime control of findividufl prosthetic ffingers. Our decodfing approach can aalso be used for the control of exoskeleton hands to assfis findividufls wfh hand impafiment. In future work, we wffl extend the

current work to decode aifl five dfigits, especiaflly the thumb movement, whfch wffl aiflflow us to evalfuate the decodfing method in functfional tasks ifinoflfing object manufuflatfions. Second, it is important to note that the data from different sources often exhibf heterogeneity and may not follow the assumption of being findependent and ifentificaly dfistrifuted (i.e., i.d.). Thhis rafises concerns about the robustness of our deep learning modefl when applied to diverse applicafion scenarios. Therefore, it is crucial to thoroughly evalfuate and examine the robustness of our modefl across varfious real-world scenarios, taking into account the potential varfations and chafiflenges present in the data [50]. The current study only evalfuated intact findividufls, future work wffl investigate the performance of the decoder on amputees, whfch is more chafiflenging since there wffl be a flfimf on the length of residual arm needed for the HD-EMG electrode placement. In addfition, the muscle recruitment patterns may aalso change due to amputation. As a result, further optimifization of the neuralf decoder may be needed to consider different muscle activfation patterns of different amputee subjects. Lastfily, the current CNN modefl is a black-box approach, and we do not have dfirect finformation regarding what finformation were extracted by the modefl. It is crucial to investigate the explainability of the proposed modefl before impflementation in practical applications [50].

In conclusion, thhis study impflemented a deep neuralf network as a robust and effficient neuralf decodfing method to predict popuflatfion neuron ffirfing frequency (i.e., neuralf drfive) from sfingle finger movements. The predicted neuralf drfive was then used to control sfingle-finger or mufltfi-finger movements of a robotic hand in a real-ttime manner. Our results showed that the extracted MU ffirfing frequency finformation can lead to accurate and robust predictions of jofint angles, compared wfh the HD-EMG ampfitude method. Further development of thhis decodfing method can potentially provide a reliable neuralf-machfne finteface that can continuously decode findividufl finger movements for fintutifive control of robotic hands wfh hffig movement dexterity.

Declaration of competing interest

None declared.

Acknowledgement

Thhis study was supported in part by the National Science Foundation (CBET-1847319, IIS-2106747) and the Department of Defense (W81XWH2110185).

Appendix A. Supplementary data

Supplementary data to thhis article can be found onlfine at <https://doi.org/10.1016/j.combiomed.2023.107139>.

References

- C. Castellfifini, "Upper Limb Active Prosthetic Systems—Overview," *Wearable Robotics*, Academic Press., 2020, pp. 365–376.
- M.S. Johannes, E.L. Faullfing, K.D. Katyafl, M.P. Para, J.B. Heflder, A. Makhlifin, T. Moyer, D. Wahlf, J. Soflberg, S. Clark, R.S. Armfiger, "The Moduflar Prosthetic Limb," *Wearable Robotics*, Academic Press, 2020, pp. 393–444.
- T.T. Worsnopp, M.A. Peshkfin, J.E. Cofigate, D.G. Kamper, An actuated finger exoskeleton for hand rehabilitation following stroke, in: 2007 IEEE 10th International Conference on Rehabilitation Robotics, vols. 1 and 2, 2007, pp. 896–.
- K.Y. Tong, S.K. Ho, P.K. Pang, X.L. Hu, W.K. Tam, K.L. Fung, X.J. Wei, P.N. Chen, M. Chen, An fintentfion driven hand functions task trafining robotic system, *Conf Proc IEEE Eng Med Biol Soc* 2010 (2010) 3406–3409.
- C. Castellfifini, P. Artemiaflis, M. Wffifinger, A. Ajoudanfi, M. Afifimusaj, A. Bicchfi, B. Caputo, W. Craeflfis, S. Dosen, K. Englehart, D. Farfina, A. Gfifsbets, S.B. Godfrey, L. Hargrove, M. Ison, T. Kuflken, M. Markovic, P.M. Pfiflarski, R. Rupp, E. Scheme, Proceedings of the first workshop on Peripheraf Machfne Interfaces: going beyond traditionalif surface electromyography, *Front. Neurorob.* 8 (2014) 22.
- J. Stefin, K. Narendran, J. McBean, K. Krebs, R. Hughes, Electromyography-controlled exoskeleton upper-limb-powered orthofis for exercise trafining after stroke, *Am. J. Phys. Med. Rehabil.* 86 (4) (Apr, 2007) 255–261.

[7] A. Flemming, N. Stafford, S. Huang, X. Hu, D.P. Ferris, H. Huang, Myoelectric control of robotic finger limb prostheses: a review of electromyography interfaces, control paradigms, challenges and future directions, *J. Neurosci. Eng.* 18 (4) (2021), 041004.

[8] E.N. Kamavuako, E.J. Scheme, K.B. Englehart, Determination of optimum threshold values for EMG time domain features: a multifeature dataset investigation, *J. Neurosci. Eng.* 13 (4) (2016), 046011.

[9] L.R. Qutidamo, F. Cavrini, L. Sbermfini, F. Ruffini, L. Bifanfi, S. Serfi, G. Saggino, Support vector machines to detect physiological patterns for EEG and EMG-based human-computer interaction: a review, *J. Neurosci. Eng.* 14 (1) (2017), 011001.

[10] Z. Lu, A. Stampa, G.E. Francisco, P. Zhou, Offline and online myoelectric pattern recognition analysis and real-time control of a robotic hand after spinal cord injury, *J. Neurosci. Eng.* 16 (3) (2019), 036018.

[11] A.B. Ajiboye, R.F. Wefir, Muscle synergies as a predictive framework for the EMG patterns of new hand postures, *J. Neurosci. Eng.* 6 (3) (2009), 036004.

[12] L.H. Smith, T.A. Kuiken, L.J. Hargrove, Real-time simultaneous and proportional myoelectric control using intramuscular EMG, *J. Neurosci. Eng.* 11 (6) (2014), 066013.

[13] M. Jordanic, M. Rojas-Martinez, M.A. Mafianas, J.F. Alonso, Prediction of isometric motor tasks and effort levels based on high-density EMG in patients with incomplete spinal cord injury, *J. Neurosci. Eng.* 13 (4) (2016), 046002.

[14] I.J.R. Martinez, A. Mannini, F. Clemente, A.M. Sabatini, C. Cipriani, Grasp force estimation from the transient EMG using high-density surface recordings, *J. Neurosci. Eng.* 17 (1) (2020), 016052.

[15] J.N. Lefijse, N.H. Campbell-Kyureghyan, D. Spektor, P.M. Quesada, Assessment of individual finger muscle activity for the extensor digitorum communis by surface EMG, *J. Neurophysiol.* 100 (6) (Dec, 2008), 3225-35.

[16] L. Hargrove, K. Englehart, B. Hudgins, The effect of electrode displacements on pattern recognition based myoelectric control, *Conf Proc IEEE Eng Med Biol Soc* 1 (2006) 2203-2206.

[17] A. Hoflobar, D. Farfina, M. Gazzonfi, R. Merletti, D. Zazuza, Estimating motor unit discharge patterns from high-density surface electromyogram, *Offin Neurophysiol.* 120 (3) (Mar, 2009) 551-562.

[18] C.J. De Luca, A. Adam, R. Wotfiz, L.D. Giffmore, S.H. Nawab, Decomposition of surface EMG signals, *J. Neurophysiol.* 96 (3) (Sep, 2006), 1646-57.

[19] R. Merletti, A. Botter, A. Trofiano, E. Merlo, M.A. Mianetto, Technology and instrumentation for detection and conditioning of the surface electromyographic signal: state of the art, *Offin Biomech.* 24 (2) (Feb, 2009) 122-134.

[20] A. Hoflobar, D. Zazuza, Multichannel blind source separation using convolutional kernel compensation, *IEEE Trans. Signal Process.* 55 (9) (Sep, 2007) 4487-4496.

[21] F. Negro, S. Muceff, A.M. Castronovo, A. Hoflobar, D. Farfina, Multichannel intramuscular and surface EMG decomposition by convolutional blind source separation, *J. Neurosci. Eng.* 13 (2) (Apr, 2016), 026027.

[22] M. Chen, P. Zhou, A novel framework based on FastICA for high density surface EMG decomposition, *IEEE Trans. Neural Syst. Rehabil. Eng.* 24 (1) (Jan, 2016) 117-127.

[23] C. Dafi, X. Hu, Independent component analysis based algorithms for high-density electromyogram decomposition: systematic evaluation through simulation, *Comput. Biol. Med.* 109 (Jun, 2019) 171-181.

[24] Y. Zheng, X. Hu, Real-time isometric finger extension force estimation based on motor unit discharge information, *J. Neurosci. Eng.* 16 (6) (2019), 066006.

[25] V. Gfaser, A. Hoflobar, D. Zazuza, Real-time motor unit identification from high-density surface EMG, *IEEE Trans. Neural Syst. Rehabil. Eng.* 21 (6) (2013) 949-958.

[26] W. Wefir, Y. Wong, Y. Du, Y. Hu, M. Kankanhall, W. Geng, A multistream convolutional neural network for sEMG-based gesture recognition in muscle-computer interface, *Pattern Recogn. Lett.* 119 (2019) 131-138.

[27] W. Geng, Y. Du, W. Jin, W. Wefir, Y. Hu, J. Ili, Gesture recognition by instantaneous surface EMG images, *Sci. Rep.* 6 (Nov 15, 2016), 36571.

[28] K.-T. Kim, C. Guan, S.-W. Lee, A subject-transfer framework based on single-trial EMG analysis using convolutional neural networks, *IEEE Trans. Neural Syst. Rehabil. Eng.* 28 (1) (2020) 94-103.

[29] A. Ameri, M.A. Akhaee, E. Scheme, K. Englehart, Regression convolutional neural network for improved simultaneous EMG control, *J. Neurosci. Eng.* 16 (3) (2019), 036015.

[30] Y. Geng, Z. Yu, Y. Long, L. Qin, Z. Chen, Y. Ili, X. Guo, G. Ili, A CNN-attention network for continuous estimation of finger kinematics from surface electromyography, *IEEE Rob. Autom. Lett.* 7 (3) (2022) 6297-6304.

[31] W. Guo, C. Ma, Z. Wang, H. Zhang, D. Farfina, N. Jifang, C. Ilin, Long exposure convolutional memory network for accurate estimation of finger kinematics from surface electromyographic signals, *J. Neurosci. Eng.* 18 (2) (Mar 3, 2021).

[32] C. Wang, W. Guo, H. Zhang, L. Guo, C. Huang, C. Ilin, sEMG-based continuous estimation of grasp movements by long-short term memory network, *BioMed. Signal Process Control* 59 (2020), 101774.

[33] F. Qutifira, T. Kofike-Akfini, Y. Wang, D. Erdogmus, Translating sEMG Signals to Continuous Hand Poses Using Recurrent Neural Networks, 2018, pp. 166-169.

[34] R. Roy, F. Xu, D.G. Kamper, X. Hu, A generic neural network model to estimate population neural activity for robust neural decoding, *Comput. Biol. Med.* 144 (2022), 105359.

[35] C. Dafi, X. Hu, Independent component analysis based algorithms for high-density electromyogram decomposition: experimental evaluation of upper extremity muscles, *Comput. Biol. Med.* 108 (May, 2019) 42-48.

[36] D. Arthur, S. Vassilvitskii, k-means++: the Advantages of Careful Seeding, Stanford, 2006.

[37] Y. Ning, X. Zhu, S. Zhu, Y. Zhang, Surface EMG decomposition based on K-means clustering and convolutional kernel compensation, *IEEE J. Biomed. Health Inform.* 19 (2) (Mar, 2015) 471-477.

[38] F. Xu, Y. Zheng, X. Hu, Real-time finger force prediction via parallel convolutional neural networks: a preliminary study, *Annu Int Conf IEEE Eng Med Biol Soc* 2020 (Jul, 2020) 3126-3129.

[39] Y. Zheng, X. Hu, Concurrent estimation of finger flexion and extension forces using motoneuron discharge information, *IEEE (Inst. Electr. Electron. Eng.) Trans. Biomed. Eng.* 68 (5) (2021) 1638-1645.

[40] C. Dafi, X. Hu, Extracting and classifying spatiotemporal muscle activation patterns for forearm flexor muscles using high-density electromyogram recordings, *Int. J. Neurosci. Syst.* 29 (1) (Feb, 2019), 1850025.

[41] D.P. Kingma, J.L. Ba, Adam: A Method for Stochastic Optimization, 3rd Int. Conf. Learn. Represent., 2015.

[42] C. Dafi, X. Hu, Finger joint angle estimation based on motoneuron discharge activities, *IEEE J. Biomed. Health Inform.* 24 (3) (Mar, 2020) 760-767.

[43] Y. Zheng, X. Hu, Concurrent prediction of finger forces based on source separation and classification of neuron discharge information, *Int. J. Neural Syst.* 31 (6) (2021), 2150010.

[44] J.E. Downey, L. Brane, R.A. Gaunt, E.C. Tyller-Kabara, M.L. Bonfinger, J. L. Coffifinger, Motor cortical activity changes during neuroprosthetic-controlled object interaction, *Sci. Rep.* 7 (1) (Dec 5, 2017), 16947.

[45] P. Heo, G.M. Gu, S.J. Lee, K. Rhee, J. Kim, Current hand exoskeleton technologies for rehabilitation and assistive engineering, *Int. J. Precis. Eng. Manuf.* 13 (5) (May, 2012) 807-824.

[46] M.H. Schieber, M. Santelli, Hand function: peripheral and central constraints on performance, *J. Appl. Physiol.* 96 (6) (Jun, 2004) 2293-2300.

[47] M. Santelli, A.J. Fuglevand, Role of across-muscle motor unit synchrony for the coordination of forces, *Exp. Brain Res.* 159 (4) (Dec, 2004) 501-508.

[48] J.N. Lefijse, S. Carter, A. Gupta, S. McCabe, Anatomic basis for individualized surface EMG and homogeneous electrostimulation with neuroprostheses of the extensor digitorum communis, *J. Neurophysiol.* 100 (1) (Jul, 2008) 64-75.

[49] M. Santelli, G. Baud-Bovy, H. Jornet, Neural bases of hand synergies, *Front. Comput. Neurosci.* 7 (2013) 23.

[50] A. Hofzinger, The next frontier: AI we can really trust, in: Machine Learning and Principles and Practice of Knowledge Discovery in Databases vol. 2021, ECML PKDD, 2021, pp. 427-440.